Symmetry-based recoupling in double-rotation NMR spectroscopy

Andreas Brinkmann,[1,a] Arno P. M. Kentgens,[1] Tiit Anupõld,[2] and Ago Samoson[2]
[1]*Physical Chemistry/Solid State NMR, Institute for Molecules and Materials, Radboud University Nijmegen, P.O. Box 9010, 6500 GL Nijmegen, The Netherlands*
[2]*National Institute of Chemical Physics and Biophysics, 12618 Tallinn, Estonia*

(Received 10 July 2008; accepted 1 October 2008; published online 6 November 2008)

In this contribution, we extend the theory of symmetry-based pulse sequences of types CN_n^ν and RN_n^ν in magic-angle-spinning nuclear resonance spectroscopy [M. H. Levitt, in *Encyclopedia of Nuclear Magnetic Resonance*, edited by D. M. Grant and R. K. Harris (Wiley, Chichester, 2002), Vol. 9]. to the case of rotating the sample simultaneously around two different angles with respect to the external magnetic field (double-rotation). We consider the case of spin-1/2 nuclei in general and the case of half-integer quadrupolar nuclei that are subjected to weak radio frequency pulses operating selectively on the central-transition polarizations. The transformation properties of the homonuclear dipolar interactions and *J*-couplings under central-transition-selective spin rotations are presented. We show that the pulse sequence $R2_2^1R2_2^{-1}$ originally developed for homonuclear dipolar recoupling of half-integer quadrupolar nuclei under magic-angle-spinning conditions [M. Edén, D. Zhou, and J. Yu, Chem. Phys. Lett. **431**, 397 (2006)] may be used for the same purpose in the case of double rotation, if the radio frequency pulses are synchronized with the outer rotation of the sample. We apply this sequence, sandwiched by central-transition selective 90° pulses, to excite double-quantum coherences in homonuclear spin systems consisting of ^{23}Na and ^{27}Al nuclei. © *2008 American Institute of Physics*. [DOI: 10.1063/1.3005395]

I. INTRODUCTION

Solid-state NMR has developed into a powerful tool for obtaining detailed information about the structure, order, and dynamics in partly disordered inorganic, organic, and biological materials. Typical examples for which NMR studies are favored are glasses, micro- and mesoporous materials including zeolites and aluminophosphates, aluminates, metal hydrides, semiconductors, natural and synthetic polymers, biomimicking materials, biological macromolecules, and fibers. Qualitative and quantitative information about spatial proximity and internuclear distances may be obtained by utilizing the internuclear dipolar interactions. In order to obtain high-resolution isotropic spectra of spin-1/2 nuclei, the sample is rapidly rotated about an axis at the magic angle (≈54.74°) with respect to the static magnetic field, which largely removes the effect of anisotropic spin interactions. To establish spatial proximities and estimate internuclear distances under magic-angle spinning (MAS) conditions requires sequences of resonant radio frequency (rf) pulses synchronized with the sample rotation to suspend the averaging effect of the MAS over a defined time interval. There are many different types of pulse sequences achieving recoupling of dipolar interactions between nuclei of the same type (homonuclear recoupling) and between nuclei of different types (heteronuclear recoupling).[1–3] Especially the use of symmetry theory has led to the design of many rotor-synchronized rf pulse sequences operating under MAS in recent years, denoted CN_n^ν and RN_n^ν sequences, which selectively preserve or restore certain spin interactions while suppressing others.[3,4]

Nuclei with spin $S>1/2$ are subject to quadrupolar couplings, which cannot be averaged completely by MAS. One very successful method to obtain high-resolution isotropic spectra of quadrupolar nuclei with half-integer nuclear spin is multi-quantum MAS (MQMAS) NMR.[5,6] A technically more demanding but also more powerful method to obtain high resolution spectra of quadrupolar nuclei is double rotation (DOR) NMR (Refs. 7–11). Here the sample is spun simultaneously around two angles with respect to the external magnetic field, which leads to averaging of the quadrupolar coupling and hence to well resolved spectra. Recent developments in the design of DOR stators have overcome the technical difficulties and mechanical instabilities of early approaches.[12,13]

Recoupling the dipolar interaction between quadrupolar nuclei under MAS in a controlled and predictable fashion is a difficult task because of the complicated nuclear spin dynamics of the quadrupolar nuclei in the presence of rf fields. Therefore, one successful method to establish spatial proximities between quadrupolar nuclei is spin diffusion via abundant protons.[14,15] Other methods that do not require application rf pulses to the quadrupolar nuclei are rotational resonance (R^2) (Ref. 16) and quadrupolar-driven dipolar recoupling.[17–21] These methods achieve dipolar recoupling at specific values or a certain range of the MAS frequency. In addition, spinning the sample at an angle other than the magic-angle (off-MAS) prevents the dipolar interactions to be averaged completely.[22–24] In the case of half-integer quadrupolar nuclei, the use of weak rf fields makes it possible to

[a]Author to whom correspondence should be addressed. Electronic mail: a.brinkmann@science.ru.nl. Tel.: +31-24-3653108. FAX: +31-24-3652112.

selectively rotate the central-transition polarizations in the same fashion as for fictitious spin-1/2 nuclei[25,26] each possessing two energy levels. This has allowed to transfer some of the dipolar recoupling methods employing rf fields such as the rotary resonance (R^3) (Refs. 27 and 28) and the HORROR (Refs. 27, 29, and 30) techniques that have been developed for spin-1/2 nuclei[31,32] to the case of half-integer quadrupolar nuclei. Recently, Edén *et al.* have successfully demonstrated the use of symmetry-based rf pulse sequences to achieve homonuclear dipolar recoupling between quadrupolar nuclei[33,34] by employing supercycled versions of the $R4_4^1$ and $R6_6^2$ sequences.[35] These sequences may on the one hand be employed during the mixing time of a two-dimensional (2D) experiment to obtain 2D spectra correlating single-quantum coherences (1QC) of half-integer quadrupolar nuclei in close spatial contact.[33] On the other hand, when sandwiched between central-transition selective 90° pulses, they can be used to excite two-spin double-quantum coherences (2QC) between dipolar-coupled half-integer quadrupolar nuclei and to record 2D spectra correlating 2QC and 1QC,[34] which have the advantage over 1Q-1Q correlation spectra that 2QC between identical spin sites appear on the diagonal of the 2D spectrum. It has been shown that the supercycled $R2_2^1$ sequence leads to improved performance in the excitation of two-spin 2QC in half-integer quadrupolar spin systems.[34] In addition, Mali *et al.* have used this sequence to roughly determine the homonuclear dipolar coupling from the 2QC buildup curves, when additional information about the quadrupolar coupling and its relative orientation with respect to the dipolar coupling is known.[36] Recently, Lo and Edén presented variants of the $R2_2^1$ sequence that are significantly better compensated for resonance offsets and rf amplitude errors.[37]

So far, only spin diffusion has been used to establish spatial proximities between half-integer quadrupolar nuclei under DOR conditions.[12,38] In this contribution, we extend the concept of rotor-synchronized recoupling sequences of types CN_n^ν and RN_n^ν operating under MAS to the case of DOR. In order to develop an analytical description of these recoupling sequences using average Hamiltonian theory,[39] we assume central-transition selective rf fields at this stage.

II. CENTRAL-TRANSITION SELECTIVE SYMMETRY-BASED RECOUPLING

A. Central-transition spin Hamiltonian

Consider a multiple spin system consisting of half-integer quadrupolar S-spins to which an rf sequence is applied, where the rf field strength ω_{rf} is small compared to the quadrupolar frequency $\omega_Q = 3C_Q/(2S(2S-1))$. Here $C_Q = e^2qQ/\hbar$ is the quadrupolar coupling constant, where Q is the quadrupole moment, e is the magnitude of the electron charge, and qe is the anisotropy of the electric field gradient tensor. This allows us to restrict the analysis of the S-spin dynamics to the central transition subspace, denoted $(-1/2, 1/2)$, of the quadrupolar nuclei. The use of fictitious spin-1/2 operators applied to the central transition of the quadrupolar spin system allows for a theoretical description that is analogous to the case of spin-1/2 nuclei.[25,26] In this case, the nutation frequency of the central transition magnetization is given by $\omega_{nut}(S) = (S+1/2)\omega_{rf}$. It should be noted, however, that in the case of powdered samples and sample spinning (MAS or DOR), the prerequisite of weak rf fields may not be fulfilled for all crystallite orientations and at all time points.

The total central-transition spin Hamiltonian is given by the sum of the Hamiltonians of the interaction with the central-transition selective rf field and the internal spin interactions Λ,

$$H^{(-1/2,1/2)}(t) = H_{rf}^{(-1/2,1/2)}(t) + \sum_{\Lambda} H^{\Lambda(-1/2,1/2)}(t). \tag{1}$$

The central-transition Hamiltonian $H^{\Lambda(-1/2,1/2)}(t)$ may be expressed as a sum of terms that transform as irreducible spherical tensors of rank l for spatial rotations and as irreducible spherical tensors of rank λ for rotations of the central-transition fictitious spin-1/2 polarizations. Hence, each term is a product of the component m of the lth rank spatial irreducible spherical tensor A^Λ, and the component μ of the λth rank central-transition irreducible spherical spin tensor operator $T^{\Lambda(-1/2,1/2)}$. The spatial and central-transition spin components are denoted A_{lm}^Λ and $T_{\lambda\mu}^{\Lambda(-1/2,1/2)}$, respectively, with the spatial quantum number m and spin quantum number μ taking the values $m=-l,-l+1,\ldots,l$ and $\mu=-\lambda, -\lambda+1,\ldots,\lambda$. The components $T_{\lambda\mu}^{\Lambda(-1/2,1/2)}$ are defined with the help of the fictitious spin-1/2 operators analogous to the case of spin-1/2 nuclei.[39,40] In the high-field approximation, the central-transition Hamiltonian in the laboratory frame is given by

$$H^{\Lambda(-1/2,1/2)}(t) = \sum_{\lambda,l} [A_{l0}^\Lambda(t)]^L c_\lambda^\Lambda(S) T_{\lambda 0}^{\Lambda(-1/2,1/2)}, \tag{2}$$

where $[A_{l0}^\Lambda(t)]^L$ is the 0th component of the spatial tensor written in the laboratory frame L. This component is obtained by transforming the spatial tensor from the principal axis system P of the respective spin interaction into L by a series of rotations. The space and central-transition spin ranks of the isotropic chemical shift is given by $l=0$, $\lambda=1$. The chemical shift anisotropy has ranks $l=2$, $\mu=1$. The isotropic homonuclear J-coupling has the space rank $l=0$. The homonuclear dipolar coupling has the space rank $l=2$. It should be noted that the transformation properties of the homonuclear isotropic J-coupling and homonuclear dipolar coupling under central-transition-selective spin rotations is *not* the same as under nonselective overall spin rotations. Table I lists the transformation properties of these two interactions under central-transition spin rotations. In contrast to the case of overall spin rotations, both interactions contain components that transform as tensors of rank 0 and 2 under central-transition spin rotations for $S>1/2$. This makes it necessary to introduce an additional constant $c_\lambda^\Lambda(S)$ in Eq. (2), that specifies the amplitudes of the terms with rank $\lambda=0$ and 2 for these two interactions between the nuclear spins denoted j and k,

$$[T_{20}^{jk}]_{(-1/2,1/2)} = c_0^{DD}(S) T_{00}^{jk(-1/2,1/2)} + c_2^{DD}(S) T_{20}^{jk(-1/2,1/2)}. \tag{3}$$

TABLE I. Properties of the homonuclear dipolar coupling and homonuclear isotropic J-coupling under spatial rotations and central-transition-selective spin rotations.

		Space part			(−1/2,1/2) spin part				
Interaction	Λ	l	F	$[A_{l0}]^F$	λ	$c_\lambda^\Lambda(S)$	$c_\lambda^\Lambda(1/2)$	$c_\lambda^\Lambda(3/2)$	$c_\lambda^\Lambda(5/2)$
Homonuclear dipolar coupling	DD	2	P	$\sqrt{6}b_{jk}$	0	$\sqrt{2}(S-1/2)(S+3/2)/3$	0	$\sqrt{2}$	$(8\sqrt{2})/3$
					2	$\{2+(S+1/2)^2\}/3$	1	2	11/3
Homonuclear isotropic J-coupling	J	0	L	$-\sqrt{3}2\pi J$	0	$\{1+2(S+1/2)^2\}/3$	1	3	19/3
					2	$\sqrt{2}(S-1/2)(S+3/2)/3$	0	$\sqrt{2}$	$(8\sqrt{2})/3$

$$[T_{00}^{jk}]_{(-1/2,1/2)} = c_0^J(S)T_{00}^{jk(-1/2,1/2)} + c_2^J(S)T_{20}^{jk(-1/2,1/2)}, \quad (4)$$

where subscript $[\ ]_{(-1/2,1/2)}$ denotes the central-transition elements of the given components of the irreducible spherical tensor operator for nonselective spin rotations. Table I gives the expressions for $c_\lambda^\Lambda(S)$ for general spin S and for the special cases of $S=1/2$, 3/2, and 5/2.

We would like to point out that the transformation properties of the homonuclear isotropic J-coupling between half-integer quadrupolar nuclei under central-transition-selective rf pulses listed in Table I allow the design of pulse sequences that generate an average Hamiltonian of the homonuclear J-coupling that is different from the original interaction in the laboratory frame. For example, a homonuclear double-quantum (2Q) J-coupling Hamiltonian could be created, which is not possible in the case of spin-1/2 nuclei or non-central-transition-selective pulses.

B. Average Hamiltonian theory under MAS

The symmetry-based CN_n^ν and RN_n^ν recoupling sequences, possible supercycles, and the theory of these schemes in first- and second-order average Hamiltonians have been discussed for the case of spin-1/2 nuclei under MAS conditions in great detail before.[3,41–48] Here we would like to first briefly outline the theoretical considerations for the application of CN_n^ν and RN_n^ν sequences employing weak central-transition-selective rf fields to half-integer quadrupolar nuclei in the case of MAS before extending the theoretical description to the case of DOR in the next section.

CN_n^ν and RN_n^ν sequences are defined by the set of three integer symmetry numbers (N,n,ν). A CN_n^ν sequence is constructed from a basic cyclic pulse element $\mathcal{C}$ of duration $\tau_C = n\tau_r/N$, where $\tau_r = 2\pi/\omega_r$ is the rotational period and ω_r is the angular spinning frequency. The CN_n^ν sequence is obtained by concatenating N phase-shifted cycles, with overall phase shifts that are incremented in steps of $2\pi\nu/N$ between consecutive cycles. A RN_n^ν sequence is built from a basic inversion pulse element $\mathcal{R}$ of duration $\tau_R = n\tau_r/N$. A second element $\mathcal{R}'$ is derived from $\mathcal{R}$ by reversing the sign of all rf phases. The RN_n^ν sequence is formed by repeating the pair $(\mathcal{R})_\phi(\mathcal{R}')_{-\phi}$ $N/2$ times, where the additional phase shift is given by $\phi = \pi\nu/N$. The duration of the whole CN_n^ν or RN_n^ν sequence is given by $n\tau_r$.

In the case of MAS, the component $[A_{l0}^\Lambda(t)]^L$ of the spatial tensor in the laboratory frame L in Eq. (2) may be written as

$$[A_{l0}^\Lambda(t)]^L = \sum_m [A_{lm}^\Lambda]^R d_{m0}^{(l)}(\beta_{RL})\exp\{-im(\alpha_{RL}^0 - \omega_r t)\}, \quad (5)$$

where $[A_{lm}^\Lambda]^R$ is the mth component of the spatial irreducible spherical tensor of rank l of the interaction Λ, written in the rotor-fixed frame R. The z-axis of this frame is inclined at the angle $\beta_{RL} = \arctan\sqrt{2} \approx 54.74°$ with respect to the static magnetic field direction for exact MAS and α_{RL}^0 defines the initial rotor position. The component of the spatial tensor in the rotor-fixed frame is obtained by transforming it from the principal axis system P as follows:

$$[A_{lm}^\Lambda]^R = \sum_{m',m''=-l}^{l} [A_{lm''}^\Lambda]^P D_{m''m'}^{(l)}(\Omega_{PM}^\Lambda) D_{m'm}^{(l)}(\Omega_{MR}). \quad (6)$$

The Euler angles $\Omega_{PM}^\Lambda = \{\alpha_{PM}^\Lambda, \beta_{PM}^\Lambda, \gamma_{PM}^\Lambda\}$ describe the relative orientation of the principal axis frame of the interaction Λ and a molecule-fixed frame. The Euler angles $\Omega_{MR} = \{\alpha_{MR}, \beta_{MR}, \gamma_{MR}\}$ relate the molecular frame to the rotor-fixed frame and occur with equal probability in a powder.

The rotor-synchronized CN_n^ν and RN_n^ν sequences maybe analyzed by transforming the central-transition Hamiltonian in Eq. (1) into the interaction frame of the central-transition selective rf field and by subsequently calculating the time-independent effective Hamiltonian using the Magnus expansion.[39] This approach is strictly only valid in case the rf pulses rotate the nuclear spin states in all crystallite orientations and rotor positions equally. This is fulfilled in the case of spin-1/2 nuclei, but may not be always fulfilled for spin $>1/2$ nuclei. The first order result of the effective Hamiltonian (first order average Hamiltonian) is

$$\bar{H}^{(-1/2,1/2)} = \sum_{\Lambda,l,m,\lambda,\mu} \bar{H}_{lm\lambda\mu}^{\Lambda(-1/2,1/2)} = \sum_{\Lambda,l,m,\lambda,\mu} \bar{\omega}_{lm\lambda\mu}^\Lambda c_\lambda^\Lambda(S) T_{\lambda\mu}^{\Lambda(-1/2,1/2)}, \quad (7)$$

where

$$\bar{\omega}_{lm\lambda\mu}^\Lambda = S_{lm\lambda\mu}\kappa_{lm\lambda\mu}[A_{lm}^\Lambda]^R\exp\{-im(\alpha_{RL}^0 - \omega_r t_0)\}, \quad (8)$$

where $\kappa_{lm\lambda\mu}$ is the scaling factor[3,44,46] of the recoupled term with quantum numbers (l,m,λ,μ). The starting time point of the recoupling sequence is given by t_0 and α_{RL}^0 denotes the initial position of the MAS rotor at that time point. The factor $S_{lm\lambda\mu}$ only depends on the quantum numbers (l,m,λ,μ) and the symmetry numbers (N,n,ν) of the pulse sequence.[48] It gives rise to the first order selection rules,[3,41,43,45,48] i.e., it evaluates to $S_{lm\lambda\mu}=1$, except in the cases

$$\bar{H}_{lm\lambda\mu}^{\Lambda(-1/2,1/2)} = S_{lm\lambda\mu} = 0 \quad \text{if} \quad \begin{cases} mn - \mu\nu \neq NZ & \text{for } CN_n^\nu \\ mn - \mu\nu \neq \frac{N}{2}Z_\lambda & \text{for } RN_n^\nu. \end{cases} \tag{9}$$

Here Z is any integer and Z_λ is an integer with the same parity as λ. For even λ, Z_λ represents any *even* integer, whereas it corresponds to any *odd* integer if λ is odd.

C. Average Hamiltonian theory under DOR

In the following, we extend the case of symmetry-based recoupling to the case of DOR following the discussion of the MAS case in the previous section. We define $\tau_{or} = 2\pi/\omega_{or}$ and $\tau_{ir} = 2\pi/\omega_{ir}$ as the periods and ω_{or} and ω_{ir} as the spinning frequencies of the rotation of the outer and inner rotor, respectively. In order to be able to apply average Hamiltonian theory, we assume for simplicity that the ratio of the two spinning frequencies corresponds to a rational number,

$$p_{ir}\tau_{ir} = p_{or}\tau_{or} = T_r, \tag{10}$$

$$p_{ir}\omega_{or} = p_{or}\omega_{ir}, \tag{11}$$

where p_{ir} and p_{or} are relative prime integers. The rotation of the outer and inner rotor therefore share the same period T_r. It should be noted that alternatively Floquet theory[49–52] could be used to analyze recoupling by rf pulse sequences under DOR. This approach does not require the assumption Eq. (11), i.e., the two rotation frequencies may be incommensurate. The case of DOR experiments without the application of rf pulses has been described using bimodal Floquet theory,[52–54] whereas in case that rf irradiation is applied with an additional incommensurate periodicity, a trimodal approach is required.[50,55]

We would like to define symmetry-based pulse sequences under DOR in a similar way as it is done under MAS described in Sec. II B. However, since in general we have to use the common period T_r as reference instead of solely the inner or outer rotation period, we suggest to use a different notation for the pulse sequences under DOR. $\tilde{C}\tilde{N}_n^{\tilde{\nu}}(p_{ir}/p_{or})$ and $\tilde{R}\tilde{N}_n^{\tilde{\nu}}(p_{ir}/p_{or})$ sequences under DOR are constructed by placing a total of $\tilde{N}$ basic elements in np_{or} periods of the rotation of the outer rotor, which corresponds to np_{ir} periods of the inner rotation, as shown by Eq. (10). The symmetry number $\tilde{\nu}$ has the same function to define the phases of the basic elements as ν for the case of MAS, i.e., the phases are incremented in steps of $2\pi\tilde{\nu}/\tilde{N}$ in case of $\tilde{C}\tilde{N}_n^{\tilde{\nu}}(p_{ir}/p_{or})$ sequences, and the additional phase shift is given by $\phi = \pi\tilde{\nu}/\tilde{N}$ in case of $\tilde{R}\tilde{N}_n^{\tilde{\nu}}(p_{ir}/p_{or})$ sequences. Figure 1 shows an example to illustrate this notation.

In the case of DOR, the component $[A_{l0}^\Lambda(t)]^L$ of the spatial tensor in the laboratory frame L in Eq. (2) may be written as

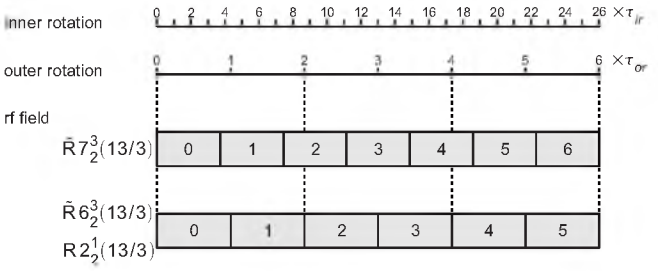

FIG. 1. Examples to illustrate the notation of the rotor-synchronized pulse sequences under DOR for $p_{ir}/p_{or}=13/3$. In the case of the $\tilde{R}7_2^3(13/3)$ sequence ($\tilde{N}=7$, $n=2$, $\tilde{\nu}=3$), seven inversion elements are placed in $np_{or}=6$ outer rotation periods corresponding to $np_{ir}=26$ inner rotation periods. The additional phase shift is given by $\phi = 180° \times \tilde{\nu}/\tilde{N} \approx 77.1°$. In the case of the $\tilde{R}6_2^3(13/3)$ sequence ($\tilde{N}=6$, $n=2$, $\tilde{\nu}=3$), six inversion elements are placed in $np_{or}=6$ outer rotation periods corresponding to $np_{ir}=26$ inner rotation periods. The additional phase shift is given by $\phi = 180° \times \tilde{\nu}/\tilde{N} = 90°$. Since for the $\tilde{R}6_2^3(13/3)$ sequence $\tilde{N}=2\times p_{or}$ and $\tilde{\nu}=1\times p_{or}$, the sequence may be defined by only referring to the outer rotation as $R2_2^1(13/3)$ with $N=2$, $n=2$, and $\nu=1$. Hence the additional phase shift is $\phi = 180° \times \nu/N = 90°$ as in the case of the corresponding sequence under MAS.

$$[A_{l0}^\Lambda(t)]^L = \sum_{m_{ir},m_{or}} [A_{lm_{ir}}^\Lambda]^I d_{m_{ir}m_{or}}^{(l)}(\beta_{IO}) d_{m_{or}0}^{(l)}(\beta_{OL}) \times \exp\{-im_{ir}(\alpha_{IO}^0 - \omega_{ir}t) - im_{or}(\gamma_{IO} + \alpha_{OL}^0 - \omega_{or}t)\}. \tag{12}$$

$[A_{lm_{ir}}^\Lambda]^I$ is the m_{ir}th component of the spatial tensor in the reference frame fixed on the inner rotor such that the z-axis points along the spinner axis of the inner rotor. The z-axis of this frame encloses an angle of $\beta_{IO} = \arctan\sqrt{4-2\sqrt{10/3}} \approx 30.56°$ with the z-axis of the reference frame fixed on the outer rotor. The z-axis of the outer-rotor frame is inclined at the magic-angle $\beta_{OL} = \arctan\sqrt{2} \approx 54.74°$ with respect to the static magnetic field direction. The angles α_{IO}^0 and α_{OL}^0 define the initial positions of the inner and outer rotor, respectively. The latter can equivalently be specified by the angle γ_{IO}, which is included in Eq. (12) for consistency with existing literature.[8,56] The component of the spatial tensor in the inner-rotor frame is obtained by transforming it from the principal axis system P,

$$[A_{lm_{ir}}^\Lambda]^I = \sum_{m',m''=-l}^{l} [A_{lm''}^\Lambda]^P D_{m''m'}^{(l)}(\Omega_{PM}^\Lambda) D_{m'm_{ir}}^{(l)}(\Omega_{MI}), \tag{13}$$

where the Euler angles $\Omega_{MI} = \{\alpha_{MI}, \beta_{MI}, \gamma_{MI}\}$ relate the molecular frame to the inner-rotor frame.

The first-order average Hamiltonian of the central-transition selective $\tilde{C}\tilde{N}_n^{\tilde{\nu}}(p_{ir}/p_{or})$ and $\tilde{R}\tilde{N}_n^{\tilde{\nu}}(p_{ir}/p_{ir})$ sequences under DOR conditions may be written as

$$\bar{H}^{(-1/2,1/2)} = \sum_{\Lambda,l,m_{ir},m_{or},\lambda,\mu} \bar{H}_{lm_{ir}m_{or}\lambda\mu}^{\Lambda(-1/2,1/2)} = \sum_{\Lambda,l,m_{ir},m_{or},\lambda,\mu} \bar{\omega}_{lm_{ir}m_{or}\lambda\mu}^\Lambda c_\lambda^\Lambda(S) T_{\lambda\mu}^{\Lambda(-1/2,1/2)}, \tag{14}$$

with

TABLE II. Scaling factors (strictly only for spin-1/2 nuclei) for the $R2_2^1R2_2^{-1}$ sequence under MAS for the basic element $(\tau_R-\tau_{180})/2-180_0-(\tau_R-\tau_{180})/2$ with $\tau_{180}=f\tau_R$.

Scaling factor	f	$f=0$	$f=1$	$f=0.1$	$f=0.067$
κ_{2120}	$\sqrt{3}\sin(\pi f)/\{4\pi(1-f^2)\}$	0	$\sqrt{3}/8\approx 0.217$	0.043	0.029
κ_{2220}	$-\sqrt{6}\sin(2\pi f)/\{16\pi(1-4f^2)\}$	0	0	−0.030	−0.020

$$\bar{\omega}^{\Lambda}_{lm_{ir}m_{or}\lambda\mu}=S_{lm_{ir}m_{or}\lambda\mu}\kappa_{lm_{ir}m_{or}\lambda\mu}[A^{\Lambda}_{lm_{ir}}]^{I}\times\exp\{-im_{ir}(\alpha^{0}_{IO}-\omega_{ir}t_0)-im_{or}(\gamma_{IO}+\alpha^{0}_{OL}-\omega_{or}t_0)\},\tag{15}$$

where $\kappa_{lm_{ir}m_{or}\lambda\mu}$ is the scaling factor of the recoupled term with quantum numbers $(l,m_{ir},m_{or},\lambda,\mu)$ and t_0 is the starting time point of the recoupling sequence. As discussed in the previous section, these results are strictly only valid in case the rf pulses rotate the nuclear spin states in all crystallite orientations and rotor positions equally. The factor $S_{lm_{ir}m_{or}\lambda\mu}$ gives rise to the first order selection rules analogous to the case of MAS, i.e., it evaluates to $S_{lm_{ir}m_{or}\lambda\mu}=1$, except in the cases

$$\bar{H}^{\Lambda}_{lm_{ir}m_{or}\lambda\mu}=S_{lm_{ir}m_{or}\lambda\mu}=0 \quad \text{if} \quad \begin{cases}(m_{ir}p_{ir}+m_{or}p_{or})n-\mu\tilde{\nu}\neq\tilde{N}Z & \text{for } \bar{C}\tilde{N}^{\tilde{\nu}}_{n}(p_{ir}/p_{or})\\ (m_{ir}p_{ir}+m_{or}p_{or})n-\mu\tilde{\nu}\neq\dfrac{\tilde{N}}{2}Z_{\lambda} & \text{for } \bar{R}\tilde{N}^{\tilde{\nu}}_{n}(p_{ir}/p_{or}).\end{cases}\tag{16}$$

Here Z is any integer and Z_λ is an integer with the same parity as λ. For even λ, Z_λ represents any *even* integer, whereas it corresponds to any *odd* integer if λ is odd.

Since the outer rotation in DOR corresponds to the magic-angle rotation, it is useful to consider the special cases, where the pulse sequence symmetries are chosen such that $\tilde{N}=Np_{or}$ and $\tilde{\nu}=\nu p_{or}$. In this special case, the symmetries can be simplified and defined by solely referring to the outer (MAS) rotation. We suggest in this case to use the plain notation $CN^{\nu}_{n}(p_{ir}/p_{or})$ and $RN^{\nu}_{n}(p_{ir}/p_{or})$, where the symmetry numbers N, n, and ν refer to the rotation of the outer rotor and make them equivalent to the definition of CN^{ν}_{n} and RN^{ν}_{n} sequences for the case of MAS, i.e., a total of N basic elements are placed in n outer rotation periods, where the phases are incremented in steps of $2\pi\nu/N$ in case of $CN^{\nu}_{n}(p_{ir}/p_{or})$ sequences, and the additional phase shift is given by $\phi=\pi\nu/N$ in case of $RN^{\nu}_{n}(p_{ir}/p_{or})$ sequences. Figure 1 shows an example of how the general notation $\bar{R}\tilde{N}^{\tilde{\nu}}_{n}(p_{ir}/p_{or})$ is linked to the simplified notation $RN^{\nu}_{n}(p_{ir}/p_{or})$ if the above conditions are fulfilled. In this case, the selection rules in Eq. (16) simplify to

$$\bar{H}^{\Lambda}_{lm_{ir}m_{or}\lambda\mu}=S_{lm_{ir}m_{or}\lambda\mu}=0, \quad \text{if} \quad \begin{cases}(m_{ir}p_{ir}/p_{or}+m_{or})n-\mu\nu\neq NZ & \text{for } CN^{\nu}_{n}(p_{ir}/p_{or})\\ (m_{ir}p_{ir}/p_{or}+m_{or})n-\mu\nu\neq\dfrac{N}{2}Z_{\lambda} & \text{for } RN^{\nu}_{n}(p_{ir}/p_{or}),\end{cases}\tag{17}$$

where it is important to note that pulse sequences $CN^{\nu}_{n}(p_{ir}/p_{or})$ and $RN^{\nu}_{n}(p_{ir}/p_{or})$ that select terms with $m_{ir}=0$ in the first order average Hamiltonian under DOR can be considered completely equivalent to their counterparts under MAS. In addition, in this case, the first order average Hamiltonian in Eqs. (14) and (15) would be independent of the initial position of the inner rotor.

D. Double-quantum recoupling under MAS

Edén *et al.* have shown that the pulse sequence $R2_2^1R2_2^{-1}$ generates a first-order average Hamiltonian containing both zero-quantum (ZQ) and 2Q terms in the homonuclear dipolar couplings[34] under MAS. A simple choice for the basic element $\mathcal{R}$ is a 180° pulse with rf phase 0 (denoted as 180_0 pulse) and the duration τ_{180} placed in the center of the time interval τ_R, where $f=\tau_{180}/\tau_R$ defines the ratio of the durations of the pulse and the basic element.[57] In the case of $f=1$, a windowless basic element is obtained, whereas the case of $f=0$ corresponds to ideal infinitesimal short pulses. In the case of a windowed or windowless basic element employing a 180_0 pulse, the recoupled terms for the homonuclear dipolar couplings under the $R2_2^1R2_2^{-1}$ sequence are given by $(l,m,\lambda,\mu)=(2,\pm2,2,0)$, $(2,\pm2,2,-2)$, $(2,\pm2,2,2)$, $(2,\pm1,2,0)$, $(2,\pm1,2,-2)$, and $(2,\pm1,2,2)$. In addition, the symmetry allowed terms for the isotropic J-couplings are given by $(l,m,\lambda,\mu)=(0,0,0,0)$, $(0,0,2,0)$, and $(0,0,2,\pm2)$, where the terms with $\lambda=2$ only appear for the case of $S>1/2$ and are a consequence of the central-transition selective rf irradiation, as shown in Table I. Therefore the total first-order central-transition average Hamiltonian for the $R2_2^1R2_2^{-1}$ is given by

$$\bar{H}^{(-1/2,1/2)}(R2_2^1R2_2^{-1})=\sum_{j<k}\{\bar{H}^{DD(-1/2,1/2)}_{jk}(R2_2^1R2_2^{-1})+\bar{H}^{J(-1/2,1/2)}_{jk}(R2_2^1R2_2^{-1})\},\tag{18}$$

where the sum is taken over all homonuclear spin-pairs. The average Hamiltonian of the homonuclear dipolar couplings may be simplified to

$$\bar{H}^{DD(-1/2,1/2)}_{jk}(R2_2^1R2_2^{-1})=c_2^{DD}(S)2\,\mathrm{Re}\left(\sum_{m=1}^{2}\bar{\omega}^{jk}_{2m20}\right)\times\left\{T^{jk(-1/2,1/2)}_{20}-\frac{1}{\sqrt{6}}(T^{jk(-1/2,1/2)}_{2-2}+T^{jk(-1/2,1/2)}_{22})\right\},\tag{19}$$

where the frequencies $\bar{\omega}^{jk}_{2m20}$ are defined in Eq. (8). The corresponding scaling factor κ_{2m20} are given in Table II and the constant $c_2^{DD}(S)$ is listed in Table I. These scaling factors are strictly only valid for the case of spin-1/2 nuclei. Edén has

calculated related scaling factors for windowed basic elements for 2Q recoupling RN_n^ν sequences.[57]

As discussed in Ref. 34, the $R2_2^1R2_2^{-1}$ sequence may be sandwiched between central-transition selective 90° pulses with phases 0° and 180° to convert the first-order central-transition average Hamiltonian in Eq. (19) into a pure 2Q average Hamiltonian. We denote the resulting sandwiched sequence as $(\Pi/2)R2_2^1R2_2^{-1}(\Pi/2)$,

$$\bar{H}_{jk}^{DD(-1/2,1/2)}[(\Pi/2)R2_2^1R2_2^{-1}(\Pi/2)] = -c_2^{DD}(S)4\ \mathrm{Re}\left(\sum_{m=1}^{2}\bar{\omega}_{2m20}^{jk}\right) \times\{T_{2-2}^{jk(-1/2,1/2)}+T_{22}^{jk(-1/2,1/2)}\}. \quad (20)$$

This 2Q average Hamiltonian enables direct excitation of 2QC from longitudinal magnetization, where the value of the constant $c_2^{DD}(S)$ reflects the increased dynamics of the excitation process for the case of central-transition selective recoupling for half-integer quadrupolar nuclei $S>1/2$ compared to the case of spin-1/2 nuclei.

E. Double-Quantum Recoupling under DOR

As discussed in the experimental section below, typical values for p_{ir}/p_{or} are in the order of 4.4–4.8. In the following discussion, we assume without loss of generality that the values for p_{ir}/p_{or} lie in this range, except that "resonance conditions" of the type $p_{ir}/p_{or}=L/2$ with L being an arbitrary integer are avoided. These special cases arise from the expression $m_{ir}p_{ir}/p_{or}$ in Eq. (17) that can take integer values if the p_{ir}/p_{or} resembles multiples of 1/2.

The set of $R2_2^1(p_{ir}/p_{or})R2_2^{-1}(p_{ir}/p_{or})$ sequences under DOR condition corresponds to the case of the $R2_2^1R2_2^{-1}$ sequence under MAS, i.e., synchronized with the rotation of the outer rotor. In the case that central-transition selective 180_0 pulses centered in the outer-rotation periods are used as basic elements, homonuclear dipolar recoupling is achieved, where the recoupled dipolar terms are in general given by $(l,m_{ir},m_{or},\lambda,\mu)=(2,0,\pm2,2,0)$, $(2,0,\pm2,2,-2)$, $(2,0,\pm2,2,2)$, $(2,0,\pm1,2,0)$, $(2,0,\pm1,2,-2)$, and $(2,0,\pm1,2,2)$. Analogous to the case in Sec. II D, the first-order dipolar average Hamiltonian for the $R2_2^1(p_{ir}/p_{or})R2_2^{-1}(p_{ir}/p_{or})$ sequences bracketed by central-transition selective 90° pulses is given by

$$\bar{H}_{jk}^{DD(-1/2,1/2)}[(\Pi/2)R2_2^1(p_{ir}/p_{or})R2_2^{-1}(p_{ir}/p_{or})(\Pi/2)] = -c_2^{DD}(S)4\ \mathrm{Re}\left(\sum_{m_{or}=1}^{2}\bar{\omega}_{20m_{or}20}^{jk}\right) \times\{T_{2-2}^{jk(-1/2,1/2)}+T_{22}^{jk(-1/2,1/2)}\}, \quad (21)$$

where the frequencies $\bar{\omega}_{20m_{or}20}^{jk}$ are defined in Eq. (12). The corresponding scaling factor $\kappa_{20m_{or}20}$ are related to the scaling factors in Table I by

$$\kappa_{20120}=d_{01}^{(2)}(\beta_{IO})\kappa_{2120}\approx 0.536\kappa_{2120}, \quad (22)$$

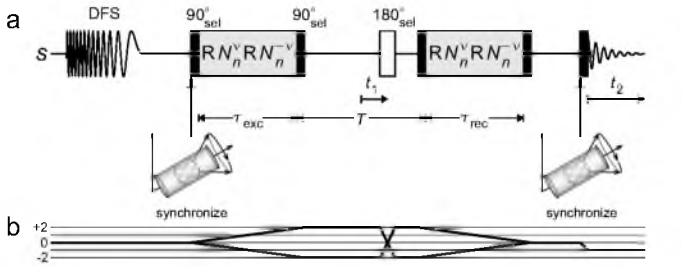

FIG. 2. (a) rf pulse sequence to record 2D homonuclear 2Q correlation spectra on half-integer quadrupolar nuclei. The subscript "sel" indicates central-transition-selective pulses. A DFS may be used to enhance the central-transition population difference. The rotor-synchronized sequence denoted $RN_n^\nu RN_n^{-\nu}$ achieves homonuclear recoupling. (b) Coherence transfer pathway diagram (Ref. 60) for the S-spins.

$$\kappa_{20220}=d_{02}^{(2)}(\beta_{IO})\kappa_{2120}\approx 0.158\kappa_{2120}. \quad (23)$$

Again, these scaling factors are strictly only valid for the case of spin-1/2 nuclei. An important property of the $R2_2^1(p_{ir}/p_{or})R2_2^{-1}(p_{ir}/p_{or})$ sequences is that solely homonuclear dipolar coupling terms with the quantum number $m_{ir}=0$ are recoupled. As a result, the central-transition first-order dipolar average Hamiltonian becomes independent of the initial position of the inner rotor. This property is essential for the experimental implementation, since it allows one to ignore the rotation of the inner rotor between the 2Q excitation and reconversion parts in the pulse sequence.

III. RESULTS AND DISCUSSION

A. Pulse sequence

As the analysis in the previous section has made clear, 2Q spectroscopy of half-integer quadrupolar nuclei under DOR conditions may be performed using the rf pulse sequence shown in Fig. 2(a) analogous to the pulse sequences operating under MAS conditions.[29,34] The sequence starts by optionally enhancing the S-spin central-transition population by a double-frequency sweep (DFS),[58] where the rf frequency has to be adiabatically swept over a subset of the satellite-transition spectral interval ensuring that the central transition is unaffected by the rf irradiation. In the following, homonuclear 2QC are excited by a central-transition selective $RN_n^\nu(p_{ir}/p_{or})RN_n^{-\nu}(p_{ir}/p_{or})$ sequence that is bracketed by central-transition 90° pulses, starting at a fixed position of the outer rotor. The excited 2QC are subjected to a Hahn echo[59] sequence of total duration T employing a central-transition selective 180° pulse as refocusing pulse in the center of the evolution time interval, which together with phase cycling allows to select the coherence transfer pathway,[60] as shown in Fig. 2(b), as two-spin and single-spin 2QC behave differently under a central-transition selective 180° pulse.[29] In case 2D 2Q spectra should be recorded the 180° pulse is shifted by an interval $t_1/2$ with respect to the center of the interval T, which has to be chosen as an integer number of outer rotation periods. Subsequently, the 2QC are reconverted into longitudinal central-transition magnetization by a second $RN_n^\nu(p_{ir}/p_{or})RN_n^{-\nu}(p_{ir}/p_{or})$ block bracketed by central-transition selective 90° pulses. Finally, observable central-transition transverse magnetization is created by a

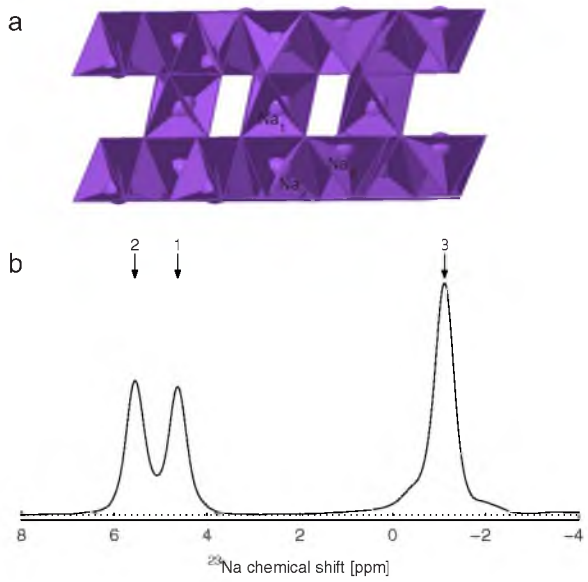

FIG. 3. (Color online) (a) Crystal structure of Na_2SO_3, where the three inequivalent Na sites are labeled (Ref. 62). (b) Experimental single-pulse ^{23}Na DOR spectrum of Na_2SO_3 at outer and inner spinning frequencies of 1803 and 8000 Hz, respectively, and at an external field of 14.1 T. The assignment of the ^{23}Na resonances according to Ref. 64 is indicated.

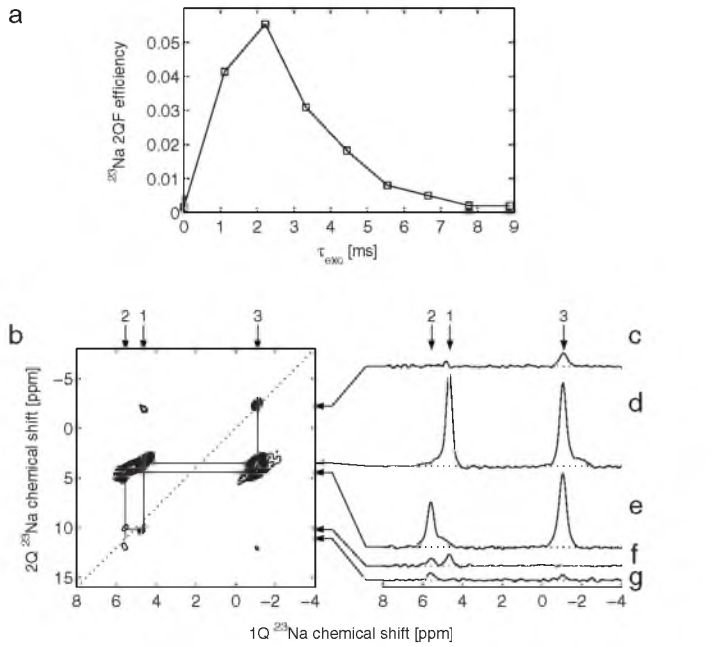

FIG. 4. (a) Experimental total ^{23}Na 2Q filtered efficiencies obtained in Na_2SO_3 as a function of $\tau_{exc}=\tau_{rec}$ recorder using the $R2_2^1(4.44)R2_2^{-1}(4.44)$ sequence at outer and inner spinning frequencies of 1803 and 8000 Hz, respectively, and at an external field of 14.1 T. The central-transition selective 90° pulses and 180° ^{23}Na pulses employed an rf field strength of $\omega_{rf}/2\pi=5.1$ kHz and no DFS was used to enhance the ^{23}Na central-transition population difference. The spin-echo time was set to two outer-rotation periods $T=1.109$ ms and for each experiment 256 transients were averaged with a relaxation delay of 1 s. (b) Experimental 2D ^{23}Na 2Q spectrum of Na_2SO_3 using $\tau_{exc}=\tau_{rec}=1.109$ ms (two outer-rotation periods). The spin-echo time was adjusted to 20 outer-rotation periods $T=11.093$ ms, and the interval t_1 was incremented in 64 steps of $\Delta t_1=166.67$ μs, where 384 transients were averaged for each t_1 increment. The other experimental parameters were identical to those given in (a).

central-transition selective 90° read pulse at a time point that corresponds to either the upward ($\alpha_{OL}^0=0$) or downward ($\alpha_{OL}^0=180°$) position of the inner rotor with respect to the external magnetic field to achieve suppression of odd-order spinning sidebands of the outer rotation during signal detection.[8,56]

The constant-time procedure in the t_1 increment prevents spinning sidebands in the corresponding indirect spectral ω_1 dimension. These sidebands will arise from the modulation of the 2Q signal amplitudes if the starting-time point of the reconversion sequence (and therefore the position of the outer rotor) is shifted as t_1 is incremented. This *rotor encoding*[61] may be avoided if the recoupling sequence is γ-encoded,[32] i.e., the 2Q signal amplitudes depend only on two of the three powder angles Ω_{MR} or Ω_{MI} for the cases of MAS or DOR, respectively.[3] However, since the $R2_2^1(p_{ir}/p_{or})R2_2^{-1}(p_{ir}/p_{or})$ sequences are not γ-encoded, rotor encoding can only be avoided by incrementing t_1 in steps of an integer number of outer-rotation periods leading to a limited spectral width in ω_1 or by the constant-time procedure used here.

All experiments were performed at static magnetic fields of 14.1 T using a Bruker Advance-II console and a homebuilt single-resonance DOR probehead utilizing air bearings for the inner rotor and employing a computer-assisted startup procedure.[12,13] We typically used spinning frequencies of 1700–1800 Hz for the outer rotor, where the ratio of the spinning frequencies of the inner and outer rotor were in the order $p_{ir}/p_{or}\approx 4.4-4.8$. The 2Q experiments were carried out on ^{23}Na and ^{27}Al at Larmor frequencies of −158.8 and −156.4 MHz, respectively. The total 2Q filtered (2QF) efficiencies were determined by integration of all 2Q signals and dividing the result by the integral of the signals in a single-pulse reference spectrum under otherwise identical experimental conditions (including the optional enhancement of the central-transition population by DFS). In order to select the 2Q coherence pathways in Fig. 2(b), the excitation block, the selective 180° pulse, and the selective 90° read pulse were phase cycled using four, eight, and four steps, respectively, leading to a 128 step phase cycle in total. 2D experiments employed the time-proportional phase incrementation procedure (TPPI).[60]

B. Experimental results

1. ^{23}Na (S=3/2)

A sample of Na_2SO_3 was chosen in a first step to experimentally investigate the potential of 2Q DOR spectroscopy in spin-3/2 systems. The crystal structure of Na_2SO_3 is shown in Fig. 3(a).[62,63] It contains three inequivalent Na sites labeled Na_1, Na_2, and Na_3 with the ratio in quantities of 1:1:2, which is reflected in the one-dimensional ^{23}Na DOR spectrum shown in Fig. 3(b). The resonances of Na_1, Na_2, and Na_3 are observed at 4.6, 5.6, and −1.1 ppm respectively, where the assignment is made according to Power.[64]

Experimental ^{23}Na two-spin 2QF efficiencies obtained in a sample of Na_2SO_3 employing the pulse sequence in Fig. 2(a) with the $R2_2^1(4.44)R2_2^{-1}(4.44)$ recoupling sequence as a function of the excitation interval $\tau_{exc}=\tau_{rec}$ are shown in Fig. 4(a). In the crystal structure of Na_2SO_3 at distances shorter than 400 pm the contacts Na_1–Na_2 (309 pm),

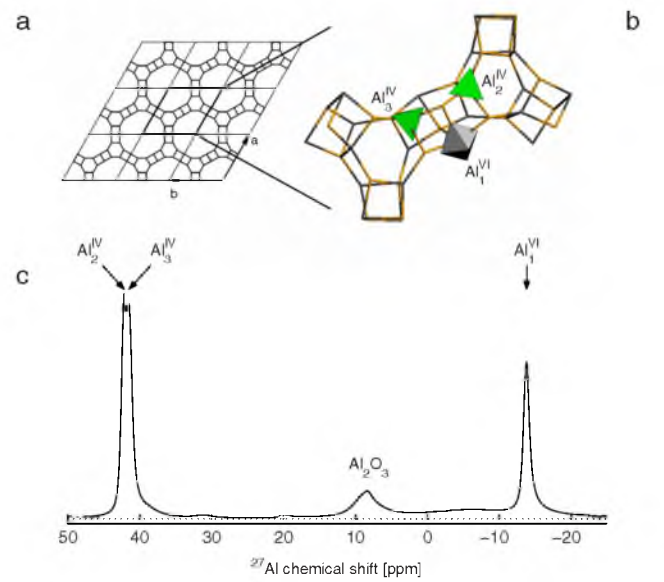

FIG. 5. (Color online) (a) Crystal structure of VPI-5, where the Al sites with tetrahedral and octahedral symmetry are indicated (Ref. 65). (b) Experimental DFS enhanced single-pulse ^{27}Al DOR spectrum of VPI-5 at outer and inner spinning frequencies of 1700 and 8020 Hz. respectively, and at an external field of 14.1 T. The assignment of the ^{27}Al resonances according to Ref. 68 is indicated. The parameters of the DFS were identical to those given in the caption of Fig. 6(a).

Na_2–Na_3 (332 pm), Na_1–Na_3 (376 pm), and Na_3–Na_3 (376 pm) can be found with the relative occurrences of 2:6:6:3. Na_1–Na_1 and Na_2–Na_2 contacts can first be found at a distance of 546 pm.[63] We obtain a maximum in the 2QF efficiency of 5.5% at an excitation time of 2.2 ms.

Figure 4(b) shows the 2D ^{23}Na DOR spectrum of Na_2SO_3 obtained at excitation and reconversion intervals of $\tau_{exc}=\tau_{rec}=1.109$ ms. The resulting 2D spectrum is well resolved in both spectral dimensions because the second-order quadrupolar broadening is removed by the DOR resulting in an isotropic 2Q spectrum comparable to 2Q spectra obtained for spin-1/2 nuclei. The resonances of sites Na_1 and Na_3 show a strong 2Q peak. The same applies to the resonances of sites Na_2 and Na_3. In addition, both the resonances of sites Na_3 and Na_2 show diagonal peaks, where the latter is relatively weak. Finally, the resonances of sites Na_1 and Na_2 show a 2Q signal with a relative small intensity compared to the Na_2–Na_3, Na_1–Na_3, and Na_3–Na_3 signals in spite of the shorter Na_1–Na_2 distance because of the much lower occurrence of this type of internuclear contact. Although both the Na_1–Na_1 and Na_2–Na_2 distances are 546 pm, only the weak Na_2–Na_2 diagonal 2Q peak could be observed in the 2D spectrum.

2. ^{27}Al (S=5/2)

In a second step, we chose a sample of the aluminophosphate VPI-5 to investigate 2Q DOR spectroscopy of spin-5/2 nuclei. The crystal structure of VPI-5 is shown in Fig. 5(a). It contains three distinct Al sites denoted Al_1^{VI}, Al_2^{IV}, and Al_3^{IV}, of which Al_1^{VI} has octahedral coordination, and Al_2^{IV} and Al_3^{IV} have tetrahedral coordination.[65,66] The one-dimensional DFS enhanced single-pulse ^{27}Al DOR spectrum of VPI-5 at room temperature and an external field of 14.1 T shown in Fig. 5(b) contains three resonance lines at shifts of −13.9, 41.5, and 42.0 ppm, where the latter two are largely overlapping. The resonance at −13.9 ppm stems from the octahedral Al_1^{VI} site whose quadrupolar coupling and asymmetry parameter are given by[67] $C_Q=3.4$ MHz and $\eta_Q=0.91$. The resonances at 41.5 and 42.0 ppm stem from the tetrahedral sites Al_3^{IV} and Al_2^{IV}, respectively, following the assignment by Grobet *et al.*,[68] where Engelhardt has suggested the opposite assignment.[69] As pointed out in Ref. 68, the spectral separation between the resonances from Al_2^{IV} and Al_3^{IV} increases with smaller external magnetic fields due to the (second order) quadrupolar-induced shift, hence ^{27}Al DOR spectra of VPI-5 at lower external fields show better spectral resolution. However, this represents a special case and in general higher external fields lead to better resolved spectra for quadrupolar nuclei also in the case of DOR because of the larger spread in the spectral frequencies due to the isotropic chemical shifts. Although the values for C_Q and η_Q are not known for the sites Al_2^{IV} and Al_3^{IV}, the quadrupolar products $P_Q=C_Q(1+\eta_Q^2/2)^{1/2}$ have been determined[70] to be 2.8 and 1.3 MHz, respectively. The closest Al–Al distances (below 500 pm) involve the following pairs of Al sites. First, Al_1^{VI}–Al_2^{IV} connectivities at 437 and 484 pm, second Al_1^{VI}–Al_3^{IV} contacts at 448 and 471 pm, third Al_2^{IV}–Al_3^{IV} distances of 470 and 479 pm, and finally a Al_2^{IV}–Al_2^{IV} separation of 498 pm. In addition, the closest contacts of type Al_1^{VI}–Al_1^{VI} and Al_3^{IV}–Al_3^{IV} can be found at 594 and 521 pm, respectively.

Experimental ^{23}Al 2QF efficiencies obtained in a sample of VPI-5 using the $R2_2^1(4.72)R2_2^{-1}(4.72)$ recoupling sequence as a function of the excitation interval $\tau_{exc}=\tau_{rec}$ are shown in Fig. 6(a). The experimentally obtained ^{27}Al 2QF efficiency in VPI-5 is unfortunately quite low. we obtain a maximum efficiency of 0.055% at an excitation time of 1.179 ms.

The reasons for this low efficiency will be investigated in more detail in the following section. First, the combination of the slow rotation of the outer rotor together with the short 180° pulse lengths leads to very low scaling factor of the recoupled dipolar interactions. Second, the relatively weak quadrupolar interaction of site Al_3^{IV} makes it difficult to operate in the central-transition selective regime of the rf pulses for this site, hence leading to low efficiency in the excitation of 2QC involving this site. Third, the relatively large differences in chemical shift of the tetrahedral and octahedral coordinated Al sites reduce the 2QF efficiency further since the basic $R2_2^1(p_{ir}/p_{or})R2_2^{-1}(p_{ir}/p_{or})$ sequences are not well compensated for these circumstances.

Figure 6(b) shows the ^{27}Al 2D 2Q spectrum of VPI-5 obtained using the $R2_2^1(4.8)R2_2^{-1}(4.8)$ sequence for $\tau_{exc}=\tau_{rec}=1.163$ ms. In spite of the low efficiency for the excitation of 2QC, the spectrum shows clearly a 2Q peak between the sites Al_1^{VI} and mainly Al_2^{IV} but also (manifested as shoulder) Al_3^{IV}. In addition, the spectrum shows a diagonal peak for the resonances of the tetrahedral sites. Therefore, the 2D 2Q DOR spectrum is in agreement with the spatial proximities listed above of the different Al sites in VPI-5.

C. Numerical simulations

In order to understand our experimental results in greater depth and evaluate the practical potential of the homonuclear

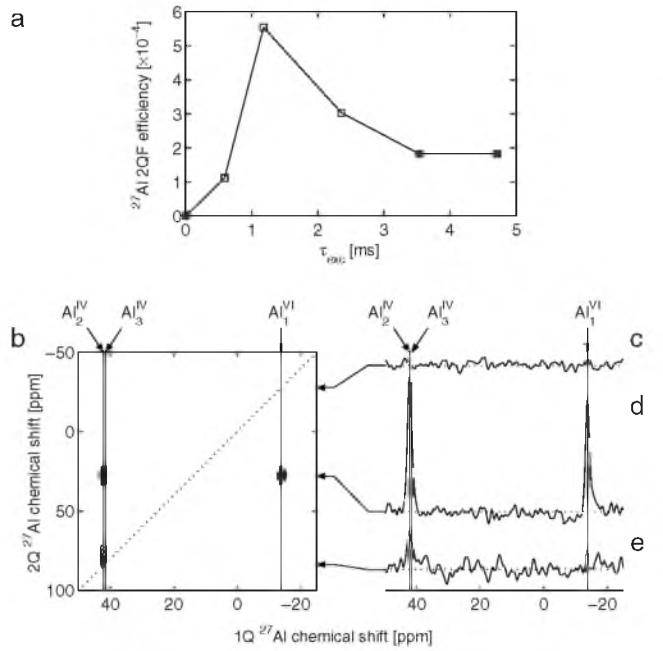

FIG. 6. (a) Experimental ^{27}Al 2Q filtered efficiencies obtained in VPI-5 as a function of $\tau_{exc}=\tau_{rec}$ obtained using the $R2_2^1(4.72)R2_2^{-1}(4.72)$ sequence at outer and inner spinning frequencies of 1700 and 8020 Hz, respectively, and at an external field of 14.1 T. The central-transition selective 90° pulses and 180° ^{27}Al pulses employed an rf field strength of $\omega_{rf}=6$ kHz and a DFS of 8 ms duration and 9 kHz rf field strength was used to enhance the ^{27}Al central-transition population difference. The spin-echo time was set to two outer-rotation periods $T=1.176$ ms and for each experiment 11 520 transients were averaged with a relaxation delay of 0.2 s. (b) Experimental 2D ^{27}Al 2Q spectrum of VPI-5 obtained using the $R2_2^1(4.8)R2_2^{-1}(4.8)$ sequence at outer and inner spinning frequencies of 1720 and 8250 Hz, respectively, and an excitation interval of $\tau_{exc}=\tau_{rec}=1.163$ ms (two outer-rotation periods). The spin-echo time was set to two outer-rotation periods and the interval t_1 was incremented in 32 steps of $\Delta t_1=21.74$ μs, where 5632 transients were averaged for each t_1 increment. The other experimental parameters were identical to those given in (a).

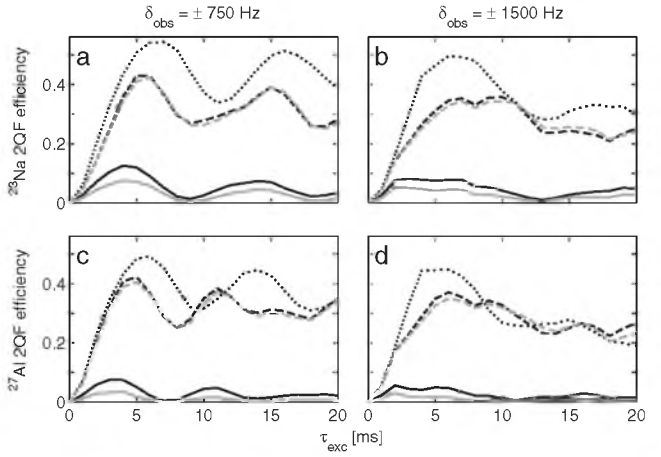

FIG. 7. Numerically simulated 2Q filtered efficiencies as a function of $\tau_{exc}=\tau_{rec}$ for the $R2_2^1(4.6)R2_2^{-1}(4.6)$ sequence at outer and inner spinning frequencies of 2000 and 9600 Hz, respectively and at an external field of 14.1 T. [(a) and (b)] Dipolar coupled two-spin $^{23}Na_1-^{23}Na_2$ system using a dipolar coupling of $b_{jk}/2\pi=-176$ Hz and an rf field strength of 7.5 kHz, and [(c) and (d)] dipolar-coupled two-spin $^{27}Al_1-^{27}Al_2$ system with a dipolar coupling of $b_{jk}/2\pi=-96$ Hz and employing an rf field with the strength of 5 kHz, hence in all cases the duration of a central-transition-selective 180° pulse is given by 33.3 μs ($f=0.067$). The isotropical chemical shifts are chosen such that the spectral peaks of $^{23}Na_1/^{23}Na_2$ and $^{27}Al_1/^{27}Al_2$ are observed at $\delta_{obs}=\pm 750$ Hz in the case of (a) and (c), and at ± 1500 Hz in the case of (b) and (d). Solid lines: Numerically exact simulations considering the first- and second-order quadrupolar couplings, the isotropic chemical shifts, and the full form of the rf Hamiltonian. Long-dashed lines: As for the solid-lines, but the rf Hamiltonian has been restricted to the central-transition part. Short-dashed lines: As for the long-dashed lines, except that the quadrupolar coupling is set to zero. In (a) and (b) the quadrupolar coupling constant and asymmetry parameter of sites $^{23}Na_1$ and $^{23}Na_2$ were set to $(C_Q/\mathrm{MHz},\eta_Q)=(3.0,0.3),(1.0,0.7)$ (black lines) and $(C_Q/\mathrm{MHz},\eta_Q)=(3.0,0.3),(0.5,0.7)$ (gray lines). In (c) and (d), the quadrupolar coupling constant and asymmetry parameter of sites $^{27}Al_1$ and $^{27}Al_2$ were set to $(C_Q/\mathrm{MHz},\eta_Q)=(6.0,0.3),(2.0,0.7)$, (black lines) and $(C_Q/\mathrm{MHz},\eta_Q)=(6.0,0.3),(1.0,0.7)$ (gray lines).

2Q recoupling of half-integer quadrupolar nuclei under DOR conditions using the $R2_2^1(p_{ir}/p_{or})R2_2^{-1}(p_{ir}/p_{or})$ sequences, we performed numerically exact simulations for dipolar coupled ^{23}Na–^{23}Na and ^{27}Al–^{27}Al two-spin systems employing the pulse sequence in Fig. 2. Figure 7 shows numerically calculated two-spin 2QF efficiencies as a function of $\tau_{exc}=\tau_{rec}$, where we studied the following three representative cases:

(i) Considering isotropical chemical shifts, but no quadrupolar couplings. In addition, the rf field Hamiltonian was restricted to the central-transition part. The results of these simulations are depicted by short-dashed lines in Fig. 7. They give a general idea about the ideal hypothetical performance of the recoupling sequence.

(ii) Considering isotropical chemical shifts, first- and second-order quadrupolar couplings, but again restricting the rf Hamiltonian to the central-transition part. The corresponding results are indicated by long-dashed lines in Fig. 7. This hypothetical case allows to evaluate the influence of the inability to employ rf pulses solely to the central transition on the efficiency to excite 2QC.

(iii) The realistic case, considering isotropic chemical shifts, first- and second-order quadrupolar couplings, and the full form of the rf Hamiltonian. The results for this case are shown as solid-lines in Fig. 7.

All simulations were performed using SIMPSON version 1.1.2 (Ref. 71) that allows to simulate DOR experiments. We added additional functions to SIMPSON that allow to restrict the rf Hamiltonian to the central-transition part and enable to set the initial rotor phases α_{IO}^0 and α_{OL}^0. In all cases, powder averaging was accomplished using a set of 1154 triplets of $\{\alpha_{MI},\beta_{MI},\gamma_{MI}\}$ angles chosen according to the Zaremba-Conroy-Wolfsberg (ZCW) scheme.[72–74] Additional parameters used for the different simulations are indicated in the caption of Fig. 7.

The simulations use outer and inner spinning frequencies of 2000 and 9600 Hz ($p_{ir}/p_{or}=4.6$), respectively, at an external field of 14.1 T. As basic element, a central-transition selective 180_0 pulse centered in the outer rotation period was chosen. All pulses except the last 90° read pulse were taken explicitly into account in the simulations. The starting and detecting density operator were set to central-transition z-magnetization. The central-transition two-spin 2QC were selected by setting all other elements in the density matrix to zero before and after the 180° spin-echo pulse. We confirmed that the simulated 2QF efficiencies are independent of the initial position α_{IO}^0 of the inner rotor.

Figure 7 is organized as follows: The first row [(a) and (b)] shows the results obtained for a dipolar coupled

two-^{23}Na-spin system with a dipolar coupling of $b_{jk}/2\pi = -176$ Hz. The rf field strength for all ^{23}Na pulses is set to 7.5 kHz. The second row [(c) and (d)] depicts the results for a dipolar coupled two-^{27}Al-spin system with a dipolar coupling of $b_{jk}/2\pi = -96$ Hz chosen scaled by a factor of $c_2^{DD}(3/2)/c_2^{DD}(5/2) = 6/11$ with a respect to the ^{23}Na–^{23}Na dipolar coupling to account for the faster dynamics of the 2Q excitation process, as shown in Eqs. (20) and (21). The rf field for all ^{27}Al pulses is adjusted to 5 kHz. Hence, both for ^{23}Na and ^{27}Al the duration of a central-transition-selective 180° pulse is given by 33.3 μs ($f = 0.067$).

The isotropic chemical shift for the simulations in the left column [(a) and (c)] was chosen such that in all cases the spectral peaks of the two sites are observed at $\delta_{\mathrm{obs}} = \pm 750$ Hz with respect to the reference frequency. In the case of the results shown in the right column [(b) and (d)], the isotropic chemical shift was adjusted such that the spectral peaks are observed at $\delta_{\mathrm{obs}} = \pm 1500$ Hz.

In addition, we studied the influence of the size of the quadrupolar coupling on the two-spin 2QC excitation efficiency. In case of the ^{23}Na simulations in (a) and (b) the black lines represent the choice of the quadrupolar coupling constant and asymmetry parameter of $\{C_Q/\mathrm{MHz}, \eta_Q\} = \{3.0, 0.3\}$ and $\{1.0, 0.7\}$ for the two sites, respectively, and the gray lines are the result of simulations in which these parameters were set to $\{C_Q/\mathrm{MHz}, \eta_Q\} = \{3.0, 0.3\}$ and $\{0.5, 0.7\}$. In case of the ^{27}Al simulations in (c) and (d), these parameters were set to $\{C_Q/\mathrm{MHz}, \eta_Q\} = \{6.0, 0.3\}, \{2.0, 0.7\}$ (black lines) and $\{C_Q/\mathrm{MHz}, \eta_Q\} = \{6.0, 0.3\}, \{1.0, 0.7\}$ (gray lines) for the two sites, respectively.

Due to the small ratio of the central-transition-selective 180° pulse and the outer rotor period of $f = 0.067$, the effective scaling factor of the recoupled homonuclear dipolar interactions in first order average Hamiltonian theory is very small, as shown in Eq. (22) and Table I. Hence, the buildup of two-spin 2QC is relatively slow as is evident from the dynamics in Fig. 7. In addition, for small f, the homonuclear recoupling is to a certain extend achieved by cross terms in second-order average Hamiltonian theory involving the homonuclear dipolar coupling and either the chemical shift or the quadrupolar coupling as can be seen by comparing the results in the left and right column of Fig. 7. This has been discussed before in the context of the homonuclear recoupling of spin-1/2 nuclei by rf-driven recoupling (RFDR),[75] finite-pulse RFDR (fpRFDR),[76] $R4_4^1$, and $R6_6^2$.[35] As a result, the dynamics of the 2Q excitation is not only sensitive to the homonuclear dipolar coupling but also depends on the chemical shifts and quadrupolar couplings of the involved nuclear sites.

An important limitation of the application of rf pulse sequences to half-integer quadrupolar nuclei is the difficulty to selectively rotate the central-transition polarizations. The simulations depicted by long-dashed black and gray lines in Fig. 7 show that more than 40% 2QF efficiencies could be achieved when only taking the central-transition part of the rf Hamiltonian into account. This value drops below 12% in case of ^{23}Na and below 8% in case of ^{27}Al when the full form of the rf Hamiltonian is considered in the simulations that are shown as solid black. This effect becomes even more evident when the quadrupolar coupling of one site is further reduced (gray lines). In this case, the maximum achieved 2QF efficiencies are reduced to below 8% in the case of ^{23}Na and below 3.5% in the case of ^{27}Al.

Furthermore, as becomes evident when comparing the results in the left column [(a) and (c)] to the results in the right column [(b) and (d)], the $R2_2^1(p_{ir}/p_{or})R2_2^{-1}(p_{ir}/p_{or})$ sequences are not well compensated for isotropic chemical shifts and rf frequency offsets. Lo and Edén have found the same property for the $R2_2^1R2_2^{-1}$ sequence under MAS condition and therefore suggested variants of this sequence to improve the compensation.[37] We are currently investigating these sequences for application under DOR condition.

As a result, for systems possessing sites with a large spread in chemical shifts and both small and large quadrupolar couplings, 2Q excitation gets considerably less efficient, since it is difficult to both operate in the central-transition-selective regime for all sites and ensure sufficient broadband excitation by the rf pulses. An alternative approach besides compensated recoupling sequences could also be to operate in the regime of strong nonselective rf pulses that can be achieved employing microcoils, which so far have been successfully combined with MAS.[77,78]

IV. CONCLUSIONS

In this contribution, we have extended the theory of symmetry based pulse sequences of types CN_n^ν and RN_n^ν operating under MAS to the case of DOR and central-transition selective pulses in systems of half-integer quadrupolar nuclei. For this purpose, the symmetry of the homonuclear dipolar interactions and J-couplings under central-transition-selective spin rotations were presented. It has been shown that the sequence $R2_2^1R2_2^{-1}$ originally developed for homonuclear dipolar recoupling of half-integer quadrupolar nuclei under MAS condition,[34] may be used for the same purpose under DOR, if the rf pulses are synchronized with the outer rotation of the sample. We have applied this sequence, sandwiched by central-transition selective 90° pulses, to excite 2QC in homonuclear spin-systems consisting of ^{23}Na and ^{27}Al nuclei. We showed that the experimental 2QF efficiencies in the case of ^{23}Na are well satisfactory to allow the broad application of 2Q ^{23}Na spectroscopy under experimental DOR conditions that are currently achievable. In the case of ^{27}Al, we found that large differences in the quadrupolar couplings and isotropic shifts of the recoupled nuclei reduce the 2QF efficiencies significantly. However, because of the superior spectral resolution of 2D 2Q DOR spectra, we see substantial potential in cases in which the distribution of chemical shifts and quadrupolar couplings is not as large, as for example in the case of ^{17}O in biological materials. Furthermore, we expect a significantly improved performance of the recoupling sequences also for the case of ^{27}Al for pulse sequences better compensated for rf offsets and future improved DOR stator designs that allow faster spinning of the outer rotor.

ACKNOWLEDGMENTS

The authors would like to thank Mattias Edén for helpful discussions, Thomas Vosegaard for pointing out to us the DOR capabilities of SIMPSON, Ernst van Eck for the VPI-5 sample, and Jan Paast for experimental help. The financial support for this research through the EuroMagNET program is acknowledged.

[1] A. E. Bennett, R. G. Griffin, and S. Vega, , in *NMR Basic Principles and Progress*, edited by P. Diehl, E. Fluck, R. Kosfeld, J. Seelig, and B. Blümich (Springer-Verlag, New York, 1984), Vol. 33.
[2] S. Dusold and A. Sebald. Annu. Rep. NMR Spectrosc. **41**, 185 (2000).
[3] M. H. Levitt, in *Encyclopedia of Nuclear Magnetic Resonance*, edited by D. M. Grant and R. K. Harris (Wiley, Chichester, 2002), Vol. 9.
[4] M. H. Levitt, J. Chem. Phys. **128**, 052205 (2008).
[5] L. Frydman and J. S. Harwood, J. Am. Chem. Soc. **117**, 5367 (1995).
[6] A. Medek, J. S. Harwood, and L. Frydman, J. Am. Chem. Soc. **117**, 12779 (1995).
[7] A. Samoson and A. Pines, Rev. Sci. Instrum. **60**, 3239 (1989).
[8] A. Samoson and E. Lippmaa, J. Magn. Reson. (1969-1992) **84**, 410 (1989).
[9] B. F. Chmelka, K. T. Mueller, A. Pines, J. Stebbins, Y. Wu, and J. W. Zwanziger, Nature (London) **339**, 42 (1989).
[10] Y. Wu, B. Q. Sun, A. Pines, A. Samoson, and E. Lippmaa, J. Magn. Reson. (1969-1992) **89**, 297 (1990).
[11] A. Samoson, in *Nuclear Magnetic Resonance in Modern Technology*, edited by G. E. Maciel (Kluwer, Dordrecht, Boston, 1994), Vol. 447.
[12] A. P. M. Kentgens, E. R. H. van Eck, T. G. Ajithkumar, T. Anupõld, J. Past, A. Reinhold, and A. Samoson, J. Magn. Reson. **178**, 212 (2006).
[13] A. P. Howes, T. Anupõld, V. Lemaitre, A. Kukol, A. Watts, A. Samoson, M. E. Smith, and R. Dupree, Chem. Phys. Lett. **421**, 42 (2006).
[14] S. Ding and C. A. McDowell, Mol. Phys. **85**, 283 (1995).
[15] N. G. Dowell, S. E. Ashbrook, and S. Wimperis, J. Phys. Chem. A **106**, 9470 (2002).
[16] M. Nijman, M. Ernst, A. P. M. Kentgens, and B. H. Meier, Mol. Phys. **98**, 161 (2000).
[17] M. J. Duer, Chem. Phys. Lett. **277**, 167 (1997).
[18] M. J. Duer and A. J. Painter, Chem. Phys. Lett. **313**, 763 (1999).
[19] M. Edén and L. Frydman, J. Chem. Phys. **114**, 4116 (2001).
[20] M. Edén, J. Grinshtein, and L. Frydman, J. Am. Chem. Soc. **124**, 9708 (2002).
[21] M. Edén and L. Frydman, J. Phys. Chem. B **107**, 14598 (2003).
[22] P. Hartmann, C. Jäger, and J. W. Zwanziger, Solid State Nucl. Magn. Reson. **13**, 245 (1999).
[23] T. G. Ajithkumar and A. P. M. Kentgens, J. Am. Chem. Soc. **125**, 2398 (2003).
[24] T. G. Ajithkumar, E. R. H. van Eck, and A. P. M. Kentgens, Solid State Nucl. Magn. Reson. **26**, 180 (2004).
[25] A. Abragam, *Principles of Nuclear Magnetism*, The International Series of Monographs on Physics, Vol. 32, 11th ed. (Oxford University Press, Oxford, 1994).
[26] S. Vega, J. Chem. Phys. **68**, 5518 (1978).
[27] M. Baldus, D. Rovnyak, and R. G. Griffin, J. Chem. Phys. **112**, 5902 (2000).
[28] S. Wi, J. W. Logan, D. Sakellariou, J. D. Walls, and A. Pines, J. Chem. Phys. **117**, 7024 (2002).
[29] G. Mali, G. Fink, and F. Taulelle, J. Chem. Phys. **120**, 2835 (2004).
[30] G. Mali and V. Kaučič, J. Magn. Reson. **171**, 48 (2004).
[31] T. G. Oas, R. G. Griffin, and M. H. Levitt, J. Chem. Phys. **89**, 692 (1988).
[32] N. C. Nielsen, H. Bildsøe, H. J. Jakobsen, and M. H. Levitt, J. Chem. Phys. **101**, 1805 (1994).
[33] M. Edén, H. Annersten, and Å. Zazzi, Chem. Phys. Lett. **410**, 24 (2005).
[34] M. Edén, D. Zhou, and J. Yu, Chem. Phys. Lett. **431**, 397 (2006).
[35] A. Brinkmann, J. Schmedt auf der Günne, and M. H. Levitt, J. Magn. Reson. **156**, 79 (2002).
[36] G. Mali, V. Kaučič, and F. Taulelle, J. Chem. Phys. **128**, 204503 (2008).
[37] A. Y. H. Lo and M. Edén, "Efficient symmetry-based homonuclear dipolar recoupling of quadrupolar spins: Double-quantum NMR correlations in amorphous solids," Phys. Chem. Chem. Phys. (in press).
[38] I. Hung, A. P. Howes, T. Anupõld, A. Samoson, D. Massiot, M. E. Smith, S. P. Brown, and R. Dupree, Chem. Phys. Lett. **432**, 152 (2006).
[39] U. Haeberlen, *High Resolution NMR in Solids: Selective Averaging*, Advances in Magnetic Resonance Suppl. 1 (Academic, New York, 1976).
[40] M. Mehring, *Principles of High Resolution NMR in Solids*, 2nd ed. (Springer-Verlag, Berlin, 1983).
[41] Y. K. Lee, N. D. Kurur, M. Helmle, O. G. Johannessen, N. C. Nielsen, and M. H. Levitt, Chem. Phys. Lett. **242**, 304 (1995).
[42] M. Hohwy, H. J. Jakobsen, M. Edén, M. H. Levitt, and N. C. Nielsen, J. Chem. Phys. **108**, 2686 (1998).
[43] M. Edén and M. H. Levitt, J. Chem. Phys. **111**, 1511 (1999).
[44] A. Brinkmann, M. Edén, and M. H. Levitt, J. Chem. Phys. **112**, 8539 (2000).
[45] M. Carravetta, M. Edén, X. Zhao, A. Brinkmann, and M. H. Levitt, Chem. Phys. Lett. **321**, 205 (2000).
[46] A. Brinkmann and M. H. Levitt, J. Chem. Phys. **115**, 357 (2001).
[47] M. Carravetta, M. Edén, O. G. Johannessen, H. Luthman, P. J. E. Verdegem, J. Lugtenburg, A. Sebald, and M. H. Levitt, J. Am. Chem. Soc. **123**, 10628 (2001).
[48] A. Brinkmann and M. Edén, J. Chem. Phys. **120**, 11726 (2004).
[49] J. H. Shirley, Phys. Rev. **138**, B979 (1965).
[50] T.-S. Ho, S.-I. Chu, and J. V. Tietz, Chem. Phys. Lett. **96**, 464 (1983).
[51] S. Vega, in *Encyclopedia of Nuclear Magnetic Resonance*, edited by D. M. Grant and R. K. Harris (Wiley, Chichester, 1996), Vol. 3.
[52] T. O. Levante, M. Baldus, B. H. Meier, and R. R. Ernst, Mol. Phys. **86**, 1195 (1995).
[53] M. Baldus, T. O. Levante, and B. H. Meier, Z. Naturforsch., A: Phys. Sci. **49**, 80 (1994).
[54] M. Baldus, B. H. Meier, R. R. Ernst, A. P. M. Kentgens, H. Meyer zu Altenschildesche, and R. Nesper, J. Am. Chem. Soc. **117**, 5141 (1995).
[55] I. Scholz, B. H. Meier, and M. Ernst, J. Chem. Phys. **127**, 204504 (2007).
[56] I. Hung, A. Wong, A. P. Howes, T. Anupõld, J. Past, A. Samoson, X. Mo, G. Wu, M. Smith, S. P. Brown, and R. Dupree, J. Magn. Reson. **188**, 246 (2007).
[57] M. Edén, Chem. Phys. Lett. **378**, 55 (2003).
[58] A. P. M. Kentgens and R. Verhagen, Chem. Phys. Lett. **300**, 435 (1999).
[59] E. L. Hahn, Phys. Rev. **80**, 580 (1950).
[60] R. R. Ernst, G. Bodenhausen, and A. Wokaun, *Principles of Nuclear Magnetic Resonance in One and Two Dimensions*, International Series of Monographs on Chemistry, Vol. 14 (Oxford University Press, Oxford, 1997).
[61] I. Schnell, Prog. Nucl. Magn. Reson. Spectrosc. **45**, 145 (2004).
[62] W. H. Zachariasen and H. E. Buckley, Phys. Rev. **37**, 1295 (1931).
[63] L. O. Larsson and P. Kierkegaard, Acta Chem. Scand. (1947-1973) **23**, 2253 (1969).
[64] W. P. Power, Magn. Reson. Chem. **33**, 220 (1995).
[65] E. G. Derouane, H. He, S. B. Derouane-Abd Hamid, and I. I. Ivanova, Catal. Lett. **58**, 1 (1999).
[66] Y. Wu, B. F. Chmelka, A. Pines, M. E. Davis, P. J. Grobet, and P. A. Jacobs, Nature (London) **346**, 550 (1990).
[67] J. Rocha, W. Kolodziejski, H. He, and J. Klinowski, J. Am. Chem. Soc. **114**, 4884 (1992).
[68] P. J. Grobet, A. Samoson, H. Geerts, J. A. Martens, and P. A. Jacobs, J. Phys. Chem. **95**, 9620 (1991).
[69] E. R. H. van Eck and W. S. Veeman, J. Am. Chem. Soc. **115**, 1168 (1993).
[70] J. Rocha, A. P. Esculcas, C. Fernandez, and J.-P. Amoureux, J. Phys. Chem. **100**, 17889 (1996).
[71] M. Bak and N. C. Nielsen, J. Magn. Reson. **147**, 296 (2000).
[72] S. K. Zaremba, SIAM Rev. **10**, 303 (1968).
[73] H. Conroy, J. Chem. Phys. **47**, 5307 (1967).
[74] V. B. Cheng, H. Henry, J. Suzukawa, and M. Wolfsberg, J. Chem. Phys. **59**, 3992 (1973).
[75] A. E. Bennett, J. H. Ok, R. G. Griffin, and S. Vega, J. Chem. Phys. **96**, 8624 (1992).
[76] Y. Ishii, J. Chem. Phys. **114**, 8473 (2001).
[77] J. W. G. Janssen, A. Brinkmann, E. R. H. van Eck, P. J. M. van Bentum, and A. P. M. Kentgens, J. Am. Chem. Soc. **128**, 8722 (2006).
[78] D. Sakellariou, G. Le Goff, and J.-F. Jacquinot, Nature (London) **447**, 694 (2007).